Nanoscale

PAPER

View Article Online
View Journal | View Issue

Check for updates

Cite this: *Nanoscale*, 2019, **11**, 15104

Halide ion influence on the formation of nickel nanoparticles and their conversion into hollow nickel phosphide and sulphide nanocrystals†

Rasmus Himstedt,[a] Dominik Hinrichs,[a] Joachim Sann,[b,c] Anica Weller,[d] Georg Steinhauser [d] and Dirk Dorfs *[a,e]

A dependence of the formation of tri-*n*-octylphosphine-capped Ni nanocrystals on the presence of halide ions during their synthesis is shown. For the application-oriented synthesis of Ni particles, this information can be crucial. Furthermore, Ni nanoparticles can be converted to nickel phosphide or sulphide by heating them up in the presence of a phosphorus or sulphur source, resulting in either solid or hollow nanocrystals, formed *via* the nanoscale Kirkendall effect, depending on the synthesis route. By adjusting the Ni crystallite size in the initial nanoparticles *via* the halide ion concentration the cavity size of the resulting hollow nanocrystals can be tuned, which is otherwise impossible to realise for particles of a similar total diameter by using this process. The synthesised hollow Ni_3S_2 nanocrystals exhibit a much sharper localised surface plasmon resonance (LSPR) band than all previously presented particles of this material, which is known to show molar extinction coefficients at the LSPR maximum similar to Au. This narrow linewidth could be explained by the nanoparticles' high crystallinity resulting from the Kirkendall process and is interesting for various possible optical applications such as surface-enhanced Raman spectroscopy owing to the low cost of the involved materials compared to the widely used noble metals.

Received 16th May 2019,
Accepted 23rd July 2019

DOI: 10.1039/c9nr04187g

rsc.li/nanoscale

Open Access Article. Published on 24 July 2019. Downloaded on 2/7/2026 11:27:34 PM.
This article is licensed under a Creative Commons Attribution-NonCommercial 3.0 Unported Licence.

Introduction

Nickel nanoparticles are currently attracting considerable interest due to their exceptional mechanical and magnetic properties.[1,2] Since it is important to meticulously control the crystallinity of the produced particles in order to reliably achieve these properties, the typical Ni nanoparticle synthesis procedures have been investigated thoroughly recently.[3,4] It is possible to synthesise various shapes of crystalline Ni nanostructures such as rods, platelets and nanocubes.[5–8] However, especially when phosphines like tri-*n*-octylphosphine (TOP), which is widely used as a capping agent for Ni nanoparticles, are present during the synthesis it can be observed that the crystallinity of the product varies and an amorphous product, consisting at least partially of nickel phosphide, is obtained depending on the reaction conditions.[9,10] So far it has for example been shown that if hydrogen gas is used as the reducing agent no amorphous particles were obtained even if phosphines were present.[8,11]

The influence of halide ions on the Ni nanocrystal formation in the presence of phosphines has however yet to be studied in detail even though for numerous other types of nanoparticle syntheses this parameter has been found to be crucial in recent years.[12,13] It is, for example, essential for the crystallisation of nanoparticles consisting of elemental metals like iron. Zhang *et al.* obtained either amorphous or crystalline Fe nanoparticles depending on the presence or absence of chloride ions during their synthesis.[14] In this work, using a slightly modified version of the basic synthesis route by Carenco *et al.* a dependence of the Ni crystallisation on the presence of halide ions, which is similar to that of the Fe system, is shown.[15] With this knowledge, it is possible to fine-tune the crystallinity of the produced Ni nanoparticles from amorphous to partially or fully crystalline just by varying the halide ion concentration in the colloidal synthesis. The reason

[a]*Institute of Physical Chemistry and Electrochemistry, Leibniz Universität Hannover, Callinstraße 3A, 30167 Hannover, Germany. E-mail: dirk.dorfs@pci.uni-hannover.de*
[b]*Center for Materials Research (LaMa), Justus Liebig University Giessen, Heinrich-Buff-Ring 16, 35392 Gießen, Germany*
[c]*Institute of Physical Chemistry, Justus Liebig University Giessen, Heinrich-Buff-Ring 17, 35392 Gießen, Germany*
[d]*Institute of Radioecology and Radiation Protection, Leibniz Universität Hannover, Herrenhäuser Straße 2, 30419 Hannover, Germany*
[e]*Cluster of Excellence PhoenixD (Photonics, Optics, and Engineering – Innovation Across Disciplines), Hannover, Germany*

† Electronic supplementary information (ESI) available: Additional TEM overview images, SAED, ICP-MS and XPS analysis of particle samples, photographs of particle dispersions in the presence of a permanent magnet, complete evaluation of syntheses with different halide or sulphur precursors, UV/vis/NIR absorbance spectra of Ni and Ni_xP_y nanoparticles. See DOI: 10.1039/c9nr04187g

This journal is © The Royal Society of Chemistry 2019

Open Access Article. Published on 24 July 2019. Downloaded on 2/7/2026 11:27:34 PM.
This article is licensed under a Creative Commons Attribution-NonCommercial 3.0 Unported Licence.

for the different degrees of crystallinity in this case however is likely a large quantity of phosphorus (up to 15 atomic%) which is incorporated into the amorphous particles during their synthesis resulting in the formation of nickel phosphide.

Furthermore, these nanoparticles can be converted to crystalline nickel phosphide particles by heating them up in the presence of a phosphorus source.[16] Nickel phosphides have recently been intensively studied due to their various possible applications as an electrocatalyst in water-splitting reactions or as the catalyst for upgrading reactions of bio-oil compounds.[17,18] The resulting nanocrystals can turn out solid or hollow depending on the chosen synthesis conditions. This study shows that the cavity size, as well as the obtained nickel phosphide phase, can also be directly controlled *via* the halide ion concentration. Amorphous, phosphorus-containing particles are converted to solid nickel phosphide crystals while previously crystalline Ni nanoparticles form hollow nanocrystals undergoing a nanoscale Kirkendall process. Transferred to heterostructures this control over the diameter of the cavities could also be interesting for applications relying on particle–particle interactions like key-lock processes, which have been demonstrated to happen on the nanoscale recently.[19]

The synthesis of hollow particles *via* the Kirkendall effect has moreover been demonstrated in case of the conversion of Ni nanoparticles to nickel oxide.[20] Thus, in this study, it is investigated whether this can be adapted to the nickel sulphide system as well. Nanostructures of the sulphide phases Ni_3S_2 (heazlewoodite) and Ni_3S_4 (polydymite) have recently been shown to exhibit localised surface plasmon resonances (LSPRs) in the visible regime of the electromagnetic spectrum with considerable molar extinction coefficients, which only a selected group of materials, mostly consisting of noble metal nanoparticles, are known to do.[21,22] The presented results show that it is indeed possible to obtain hollow nanocrystals of the aforementioned nickel sulphide phases by altering the synthesis conditions slightly. Due to their larger size and more importantly their high crystallinity resulting from the Kirkendall process, the LSPR of these nanoparticles has a narrow linewidth compared to the previously known particles of these materials.

Results and discussion

Ni nanoparticles with a diameter of roughly 16–23 nm were produced *via* the thermal decomposition of nickel acetylacetonate ($Ni(acac)_2$) in tri-*n*-octylphosphine oxide (TOPO, solvent) in the presence of tri-*n*-octylphosphine (TOP), oleylamine (OLAm) and varying amounts of halide ions. In the following, the used quantity of halide atoms is always noted as a percentage in relation to the number of Ni atoms (20% Cl^- for example means that the amount of Cl atoms is 0.2 times the amount of Ni atoms in the synthesis).

Fig. 1 shows high-resolution transmission electron microscopic (HR-TEM) brightfield images of representative nanoparticles produced in the presence of varying quantities of

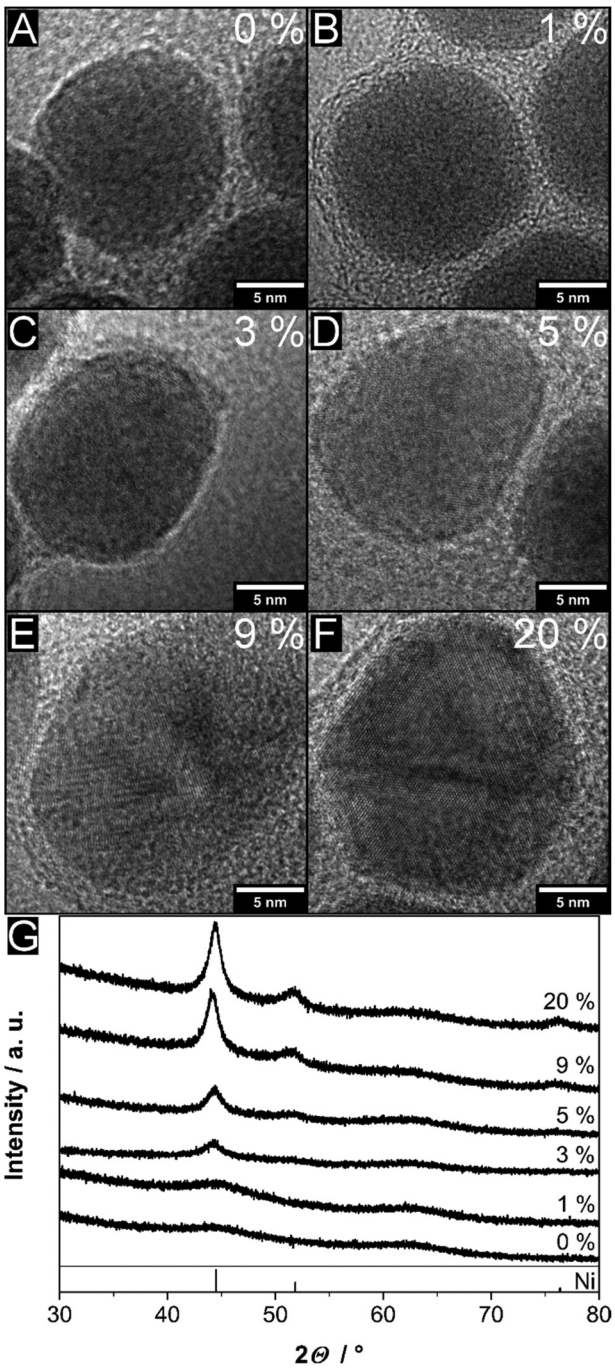

Fig. 1 High resolution TEM micrographs of nanoparticles synthesised by employing (A) 0%, (B) 1%, (C) 3%, (D) 5%, (E) 9% and (F) 20% chlorine atoms relative to nickel during the synthesis. It can be seen how the size of crystalline regions increases with larger amounts of chloride ions present. The average diameters of the shown nanoparticles are 16.3 ± 1.0 nm (A), 16.5 ± 0.7 nm (B), 16.9 ± 2.8 nm (C), 17.6 ± 1.7 nm (D), 20.0 ± 1.8 nm (E) and 22.4 ± 1.8 nm (F), respectively. TEM overview images of the respective samples can be found in Fig. S1 (ESI†). (G) X-ray diffraction patterns of the respective nanoparticle samples. While the particles are almost completely X-ray-amorphous without any chloride ions the nickel (PDF card #: 01-087-0712) crystallite size steadily increases with their concentration.

Open Access Article. Published on 24 July 2019. Downloaded on 2/7/2026 11:27:34 PM.
This article is licensed under a Creative Commons Attribution-NonCommercial 3.0 Unported Licence.

chloride ions, which are provided *via* the addition of tetradodecylammonium chloride (TDAC) to the synthesis mixture. TEM images with a lower magnification can be found in Fig. S1 in the ESI.† TDAC was chosen as the chloride precursor because it decomposes under the reaction conditions and also due to the size and therefore supposedly inactive nature of the formed cation. It can be seen that with 0% Cl^- only spherical and apparently completely amorphous particles are obtained, while with an increasing Cl^- amount larger and larger crystalline areas are visible in the nanoparticles until they appear to be fully crystalline at 9% Cl^-. Additionally, a low contrast shell around the particles, which consists of organic byproducts, can be observed.[23] In order to further investigate the crystallinity and phase of the nanoparticles, X-ray diffraction (XRD) measurements were conducted. The results are shown in Fig. 1G. It is obvious that the produced nanoparticles consist of nickel crystallites with a face-centred cubic lattice which increase in size and therefore induce sharper and more intense X-ray reflections when larger amounts of Cl^- ions are present. Additionally, the total diameter of the nanoparticles increases at a much lower rate (see Fig. S1 in the ESI†). In case of the synthesis without any chloride, only a very broad reflection, which corresponds to the Ni (1 1 1) lattice planes, at around 45°2θ can be seen. This confirms the amorphous nature of the respective nanoparticles observed during the TEM analysis. To investigate the composition of the X-ray amorphous particles three additional analysis methods were used. Selected area electron diffraction (SAED) measurements were performed as well as X-ray photoelectron spectroscopy (XPS) and inductively coupled plasma mass spectrometry (ICP-MS, see Fig. S2 in the ESI†). The results of the SAED and Ni 2p XPS experiments are typical for TOP-capped Ni nanoparticles.[23,24] However, a certain level of phosphorus doping in the Ni particles which cannot be detected by these methods is possible.[9,10,25] Indeed, P 2p XPS spectra and ICP-MS measurements show that there is a large amount of P (Ni/P molar ratio of 3.28) present in the sample containing the amorphous particles and that about 60% of the P consists of nickel phosphide, meaning that in this case, 15% of the atoms inside the particles consist of phosphorus. However, the more chloride is present during the synthesis the more the P content and the phosphide fraction thereof decreases (see Table S1 in the ESI†).

Various control experiments prove that the chloride ions are indeed the species which causes the different degree of crystallinity of the synthesised nanoparticles (see Fig. S4, S5 and their discussion in the ESI†).

Another factor which influences the growth process and final size of the obtained nanoparticles is the concentration of phosphines (TOP in this case) in the reaction mixture.[1,11,26,27] In order to ensure good comparability of all the investigated samples the TOP amount was therefore kept constant for all discussed experiments.

Furthermore, TDAC was replaced by tetradodecylammonium bromide (TDAB) to investigate whether the crystallisation of Ni can also be induced by bromide ions. TEM and XRD analysis show, that the results are again very similar (see Fig. S6 in the ESI†). Analogously to the Cl^- system, by introducing 5% Br^- to the synthesis partly crystalline particles are obtained while in case of 20% Br^- completely crystalline Ni nanoparticles are the result. The size of the obtained nanoparticles is also almost identical.

Additionally, OLAm of different purities and therefore different amounts of OLAm (see Fig. S7 and S8 in the ESI†) and a different solvent (1-octadecene instead of TOPO, see Fig. S9 in the ESI†) were employed in reference experiments to provide a better comparability of the presented results to the established literature on this type of synthesis of Ni nanoparticles.[4,15] In all investigated cases the obtained particles turned out to be amorphous without the addition of halide ions during the synthesis, while crystalline Ni nanoparticles were produced in their presence. Compared to the work by Carenco *et al.* who report a crystalline product in the absence of halide ions using pure OLAm as the solvent, the only difference of the synthesis conditions is a dilution of the reactants due to the addition of a solvent.[15] Only this dilution reveals the significant effect of halide ions on the Ni system. Furthermore and in accordance with their results, the total diameter of the Ni nanoparticles produced in this study decreases slightly when more OLAm is used. The difference between the nanoparticles synthesised in 1-octadecene and TOPO, on the other hand, is negligible (see Fig. S9†). The reason for using TOPO, which itself cannot act as a phosphorus source for the formation of nickel phosphide, is the better solubility of the particles in this solvent and the narrower size distribution of the synthesised nanoparticles.[16] Overall, the type of solvent does not seem to have a noticeable influence on the crystallinity of the Ni nanoparticles. The large amount of phosphorus contained in these particles, which leads to their amorphous character, most likely instead originates predominantly from the used TOP which, in contrast to the more stable TOPO, was present in all investigated syntheses.

Thus, it can be concluded that halide ions facilitate the crystallisation of TOP-capped fcc-Ni possibly in a way similar to the Fe nanoparticle system.[14] In the latter case, the presence of halide ions leads to the thermodynamically favoured growth of bcc-Fe nanocrystals instead of the kinetically favoured formation of amorphous Fe particles due to a larger critical radius for the nuclei caused by the ability of the halide to form complexes with metal ions and therefore dissolve the formed clusters.[14] The difference in the Ni system is however that instead of forming pure amorphous Ni nanoparticles, the kinetic control of the reaction leads to the incorporation of large amounts of P into the particles which in turn lead to their amorphous nature due to the emergence of areas of nickel phosphide. Yet, also in this case halide ions are probably able to dissolve these clusters in their *status nascendi* more easily than the presumably more thermodynamically stable crystalline Ni seeds which are therefore preferably formed in their presence. This reduction of the total number of formed stable seeds is most likely also responsible for the

 This journal is © The Royal Society of Chemistry 2019

Open Access Article. Published on 24 July 2019. Downloaded on 2/7/2026 11:27:34 PM.
This article is licensed under a Creative Commons Attribution-NonCommercial 3.0 Unported Licence.

increased size of the nanoparticles synthesised in the presence of halide ions. Alternatively, the halide ions could function as a ligand in a reaction similar to a disproportion reaction as proposed recently.[3] However, in contrast to the tendencies observed in the respective study there does not seem to be a noticeable difference between the outcomes of the additions of chloride and bromide ions in the results presented here.

The as-prepared Ni particles can be converted into nickel phosphide by further heating and annealing at higher temperatures (here 300 °C) with TOP acting as the phosphorus source.[16,28,29] HR-TEM images and XRD patterns of the so treated nanoparticles can be seen in Fig. 2 (for TEM overview images of the shown samples see Fig. S10 in the ESI†). All samples consist of highly crystalline nickel phosphide particles. Yet, it is obvious that solid particles are obtained in the absence of chloride while chloride ions lead to the formation of voids inside the nanocrystals. In combination with the results shown in Fig. 1, it can be concluded that previously crystalline regions in the Ni nanoparticles undergo a Kirkendall process and are therefore forming cavities while this process is impossible in case of amorphous precursor particles. The obtained nickel phosphide phase is $Ni_{12}P_5$ for low chloride amounts while in case of increasing chloride concentrations more and more Ni_2P is formed. One reason for this could be the low energy diffusion of P through Ni_2P.[30] The more efficient diffusion of P through this nickel phosphide phase could compete with the usually faster diffusion of Ni resulting in the preferred formation of Ni_2P compared to other phases such as $Ni_{12}P_5$. Additionally, since the P content of the Ni nanoparticles decreases with an increasing amount of used chloride, the formation of Ni_2P as the phase with a smaller Ni/P ratio could be favoured in these cases. Interestingly, also the type of halide precursor seems to have an influence on the obtained nickel phosphide phase. In the case of CTPM $Ni_{12}P_5$ can be observed exclusively while using TDAB leads to larger amounts of Ni_2P (see Fig. S4 and S6,† respectively). These two phases are generally the most likely products of this kind of synthesis while so far the synthetic lever to obtain phase pure products has been the ratio of P to Ni, the reaction temperature or time and the amount of OLAm used.[18,31,32]

Ultimately, the observed dependence of the phosphide crystallisation on the halide ion amount, which was reproduced *via* several of the aforementioned reference experiments (see Fig. S4, S6, and S7 in the ESI†), makes it possible to tune the size of the voids *via* the used halide ion concentration. In Fig. 3 its influence on the particle diameter before and after the crystallisation as well as on the resulting cavity size is summarised. It can be easily seen that while the chloride concentration does also affect the total size of the produced nanoparticles, which is probably due to a larger critical nucleation radius, the respective dependence of the void diameters is much stronger. For low halide concentrations, their size increases drastically while the total diameter of the nanoparticles stays more or less constant. For chloride amounts of above 5%, the Kirkendall process seems to be almost quantitative and the further cavity size increase is likely caused by

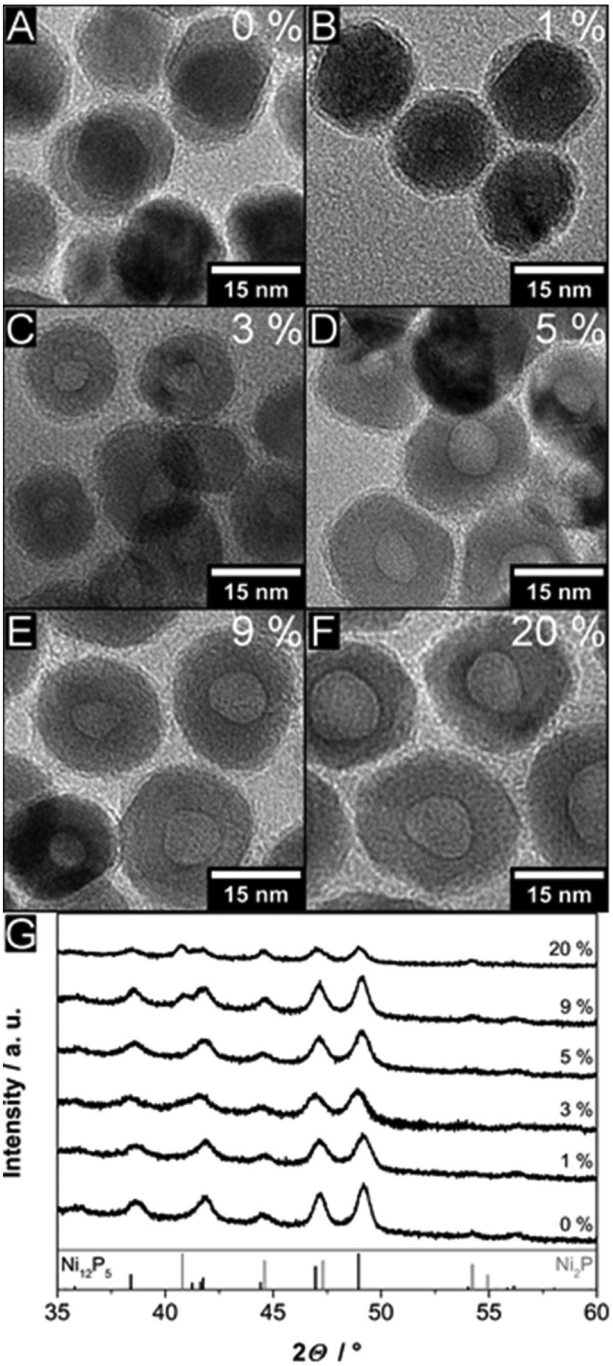

Fig. 2 High resolution TEM images of nickel phosphide nanoparticles produced by heating the previously shown Ni particles to 300 °C in the presence of TOP and (A) 0%, (B) 1%, (C) 3%, (D) 5%, (E) 9% and (F) 20% chlorine atoms relative to Ni. While solid single nanocrystals are obtained without any chloride ions, increasingly large cavities can be seen in case of larger concentrations, resulting from a nanoscale Kirkendall process. (G) X-ray diffraction patterns of the respective nanoparticle samples. The obtained crystal phase for low chloride ion concentrations is the $Ni_{12}P_5$ phase (PDF card #: 01-074-6017), while in case of high chloride amounts an increasing amount of Ni_2P (PDF card #: 00-003-0953) can be observed.

Open Access Article. Published on 24 July 2019. Downloaded on 2/7/2026 11:27:34 PM.
This article is licensed under a Creative Commons Attribution-NonCommercial 3.0 Unported Licence.

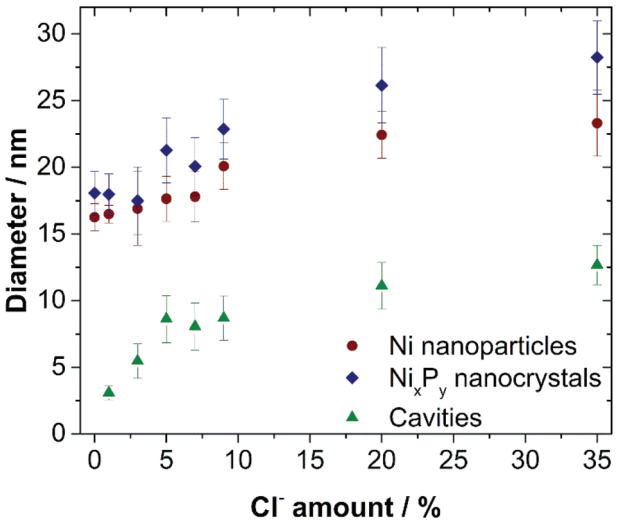

Fig. 3 Dependence of the diameter of nickel nanoparticles, the corresponding nickel phosphide nanocrystals and their inner cavity on the number of chloride ions relative to nickel atoms present during their synthesis. The error bars correspond to the standard deviations of the measured diameters. It can be seen that the overall particle size is slightly increased with larger amounts of the halide. Especially in case of low chloride concentrations however, the cavity size shows a much stronger correlation due to the strong dependence of the nickel crystallinity on the presence of the halide.

the accompanying increase in the total Ni nanoparticle diameter.

To investigate whether the above findings are also applicable to the nickel sulphide system, 1-dodecanethiol (DDT) was introduced into the synthesis as a sulphur precursor and the reaction temperature was reduced to 225 °C, which is the usual reaction temperature for the synthesis of Ni_3S_2 (heazlewoodite) and Ni_3S_4 (polydymite) nanoparticles.[21] Crystalline nickel phosphide, on the other hand, is usually not formed at this temperature.[16] In Fig. 4A–C, TEM micrographs of the produced samples are presented. It can be seen that like in the nickel phosphide system solid nanocrystals are formed without halide ions while hollow particles are obtained in their presence. The respective XRD patterns are shown in Fig. 4E. Surprisingly, in the case of 0% chloride $Ni_{12}P_5$ is formed. At this temperature this could not be achieved without adding DDT, indicating that the thiol is somehow able to activate the crystallisation of the nickel phosphide from the amorphous phosphorus-containing precursor particles at a much lower temperature than usual. However, when a chloride precursor is added Ni_3S_2 is obtained as expected. For the sample with 40% chloride, this is proven by the XRD, while in the case of the 5% sample the crystalline areas within the particles are too small to lead to visible reflections. Yet, in a representative HR-TEM image (see Fig. 4D) the Ni_3S_2 lattice planes are clearly visible. However, there is likely still a non-negligible content of nickel phosphide present in the latter particles which could be a reason for the observed small crystallite size. The respective average diameters of the precursor nano-

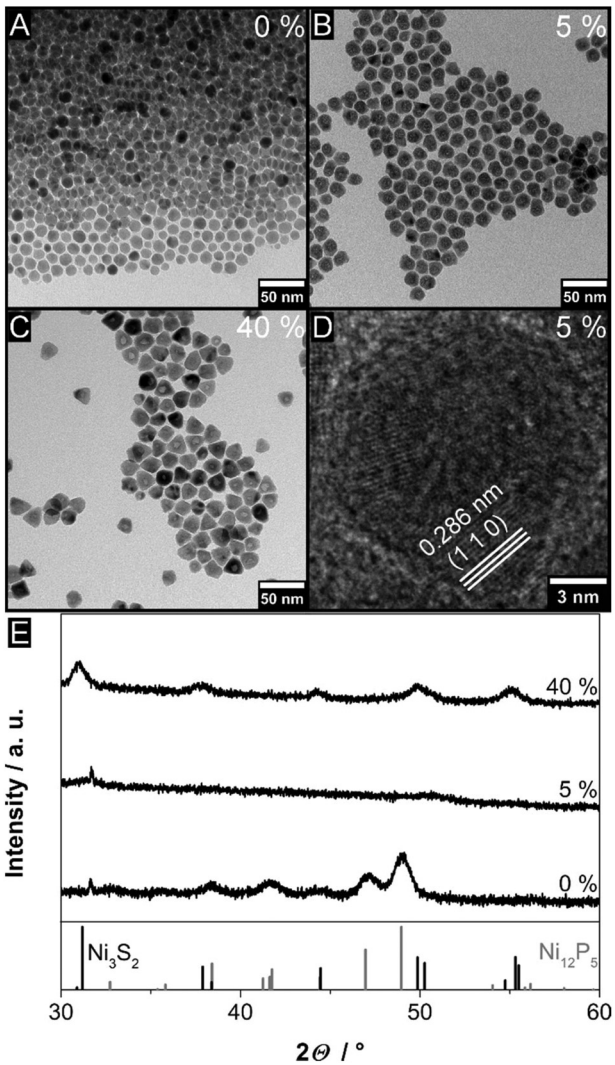

Fig. 4 TEM micrographs of nanoparticles produced by heating Ni particles to 225 °C in the presence of TOP, DDT and (A) 0%, (B) 5%, (C) 40% chlorine relative to Ni. Solid single nanocrystals are obtained without any chloride, while with an increasing amount of the halide the particles undergo a nanoscale Kirkendall effect. (D) High-resolution TEM image of a nanoparticle of the sample shown in (B). Lattice planes can be seen and were identified as the (1 1 0) planes of Ni_3S_2. (E) X-ray diffraction patterns of the presented nanoparticle samples. The obtained crystal phase for low chloride ion concentrations is the $Ni_{12}P_5$ phase (PDF card #: 01-074-6017), while in case of high chloride amounts Ni_3S_2 (PDF card #: 01-073-0698) is found. For the intermediary chloride concentration, no reflections can be observed in the XRD since the formed crystalline areas are too small.

particles as well as of the nickel sulphide nanocrystals and their inner cavities are similar to the previously shown phosphide particles and summarised in Fig. S11 (ESI†).

UV/vis/NIR absorbance spectra of the synthesised particles are shown in Fig. 5. While the spectrum of the solid nickel phosphide nanocrystals shows only a typical shoulder in the absorbance at around 500 nm (for the optical analysis of all the previously presented Ni and Ni_xP_y particles see Fig. S12 and S13,† respectively) the nickel sulphide nanoparticles exhibit an

This journal is © The Royal Society of Chemistry 2019

Open Access Article. Published on 24 July 2019. Downloaded on 2/7/2026 11:27:34 PM.
This article is licensed under a Creative Commons Attribution-NonCommercial 3.0 Unported Licence.

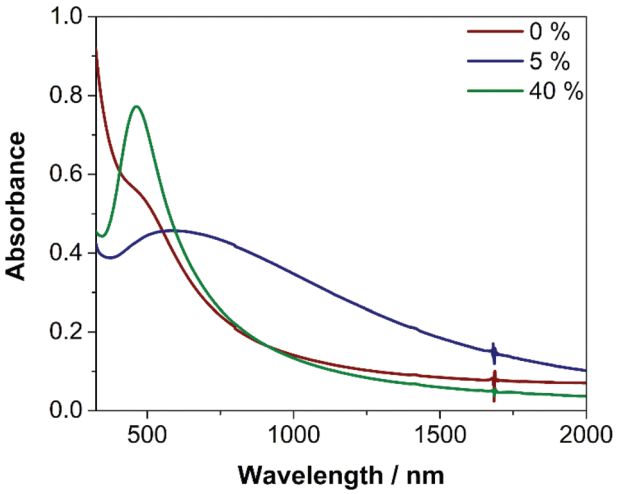

Fig. 5 UV/vis/NIR absorbance spectra of nanoparticles, which were crystallised in the presence of DDT and different chloride concentrations, in colloidal solution (toluene). It can be seen that with an increasing chloride amount an absorbance band at around 463 nm emerges, which can be attributed to the localised surface plasmon resonance of Ni_3S_2. In the case of the sample with 5% chloride, the LSPR experiences strong damping processes due to the polycrystalline nature of the nanoparticles.

absorbance band at around 463 nm which can be attributed to their localised surface plasmon resonance. Compared to previous works on plasmonic Ni_3S_2 nanoparticles the band appears at a longer wavelength and the LSPR linewidth is very narrow (full width at half maximum of roughly 200 nm compared to about 400 nm) which is most likely caused by the high degree of crystallinity of the synthesised particles due to the Kirkendall process and by their slightly larger size.[21,22]

Especially the absorbance feature of the sample with 40% chloride is very sharp. Compared to the polycrystalline 5% sample, which contains particles of a similar total diameter, or smaller Ni_3S_2 nanoparticles there is probably a lot less LSPR damping due to grain boundaries or crystal defects. This, therefore, enables the intense LSPR of the hollow nanocrystals.

It is also possible to produce hollow particles of different nickel sulphide phases by changing the sulphur precursor. If elemental sulphur dispersed in ODE is used instead of DDT hollow Ni_3S_4 nanoparticles are obtained (see Fig. S14 in the ESI†). However, in contrast to the presented Ni_3S_2 nanocrystals, these particles are polycrystalline and tend to agglomerate which leads to much broader LSPR linewidths (for a direct HR-TEM comparison of the different nickel sulphide nanoparticles see Fig. S15 in the ESI†).

Conclusions

It could be shown that the formation of TOP-capped nickel nanocrystals in colloidal solution depends on the presence of halide ions like chloride and bromide during the synthesis. Even in small amounts, the halides lead to the formation of crystalline areas within otherwise amorphous nanoparticles which also contain a large amount of phosphorus. This knowledge is important for all applications and research involving this kind of colloidal Ni particles since their degree of crystallinity can strongly influence their magnetic or optical properties and also because nickel chlorides are commonly used as precursors. Additionally, this behaviour was used to tune the size of the cavities formed within nickel phosphide and sulphide nanocrystals through a nanoscale Kirkendall effect. By the nature of this process, the diameter of these voids can otherwise not be adjusted without changing the overall size of the whole nanoparticle. This could be interesting for potential applications relying on exact cavity sizes like key–lock interactions between different nanoparticles. Also, the hollow Ni_3S_2 nanoparticles, which were synthesised for the first time on this size scale, show very promising optical properties. Their LSPR linewidth is much narrower than the one of previously known nickel sulphide nanostructures, which already show a molar extinction coefficient at the LSPR maximum, which is comparable to the values of nanoparticles consisting of noble metals like Au.[22] Thus, the presented nickel sulphide material could be a suitable low-cost alternative for the applications of plasmonic nanomaterials active in the visible regime of the electromagnetic spectrum.

Experimental section

Used chemicals

Chloroform (99%), Ni standard for AAS (1 g L^{-1}), 1-octadecene (90%, ODE), oleylamine (70%, OLAm), tetradodecylammonium bromide (99%, TDAB), tetradodecylammonium chloride (97%, TDAC), toluene (99.7%) and tri-*n*-octylphosphine oxide (99%, TOPO) were purchased from Sigma-Aldrich. Ethanol (99.8%) was purchased from Carl Roth. Nickel 2,4-pentanedionate (95%, $Ni(acac)_2$) was purchased from Alfa Aesar. Chlorotriphenylmethane (98%, CTPM), 1-dodecanethiol (98%, DDT), nickel chloride hexahydrate (99.9%, $NiCl_2{\cdot}6H_2O$) and tri-*n*-octylphosphine (97%, TOP) were purchased from abcr. Oleylamine (80–90%, OLAm) was purchased from Acros. Nitric acid trace select (69%, HNO_3) and P standard for AAS (1 g L^{-1}) were purchased from Fluka Analytical.

Synthesis of nickel nanoparticles

For the synthesis of Ni nanoparticles we used a modified version of an existing procedure by Carenco *et al.*[15] $Ni(acac)_2$ (0.1 g), TOPO (2.5 g), OLAm (80–90%, 1 mL), and a varying amount of a halide ion precursor (TDAC unless otherwise specified) were mixed in a 25 mL three-neck round-bottom flask. The mixture was degassed at 80 °C under vacuum for 2 h before TOP (0.175 mL) was added under an argon atmosphere. The reaction solution was subsequently heated up to 220 °C using a 20 °C min^{-1} heating ramp. After different time intervals samples (0.5 mL) were taken *via* a glass syringe. The usual total reaction time was 30 min. The samples were diluted with toluene (1 mL) and centrifuged (3000*g*, 10 min) after the

Open Access Article. Published on 24 July 2019. Downloaded on 2/7/2026 11:27:34 PM.
This article is licensed under a Creative Commons Attribution-NonCommercial 3.0 Unported Licence.

addition of ethanol (1 mL) before the synthesised nanoparticles were finally redispersed in toluene (1.5 mL).

Crystallisation of nickel phosphide nanoparticles

The produced nanoparticles were crystallised using a procedure similar to the two-step synthesis for nickel phosphide particles by Wang *et al.*[16] After the aforementioned 30 min at 220 °C the previously described reaction mixture was quickly heated up to 300 °C under argon atmosphere. Again samples (0.5 mL) were taken after different time intervals and the reaction was usually stopped after 30 min. The samples were purified by centrifugation (3000*g*, 10 min) after the addition of toluene (1 mL) and ethanol (1 mL) and the nanocrystals were redispersed and stored in toluene (1.5 mL).

Crystallisation of nickel sulphide nanoparticles

Nickel sulphide nanocrystals were synthesised analogously to the previously described nickel phosphide particles with the important distinctions of different amounts of $NiCl_2{\cdot}6H_2O$ substituting $Ni(acac)_2$ being the halide ion source and DDT (0.45 mL), which was added to the reaction mixture after heating up. Furthermore, the reaction temperature was reduced from 300 to 225 °C. Again, samples were taken after different times. They were purified in the same way as the nickel phosphide nanoparticles and then stored under inert conditions.

Electron microscopy

Transmission electron microscopy was performed using a Fei Tecnai G2 F20 electron microscope with a field emission gun operated at 200 kV. The nanoparticles were purified by the addition of ethanol and subsequent centrifugation (14 000*g*, 5 min). Then they were dispersed in chloroform and 10 μL of the resulting solution were drop-casted onto a carbon-coated copper grid (300 mesh) by Quantifoil.

Elemental analysis

In order to determine the mass concentrations and the present element ratios of the particle dispersions inductively coupled plasma mass spectrometry measurements were done using an Agilent 8900 mass spectrometer coupled to an autosampler SPS 4 by Agilent Technologies with the software MassHunter. For this, different aliquots of the nanoparticle samples were taken and the solvent was evaporated. The resulting precipitate was subsequently dissolved in nitric acid, further diluted with Milli-Q water in order to reach suitable mass concentrations for the respective measurement and finally measured against calibration standard solutions with known mass concentrations using a nebuliser type MicroMist. The Ni measurements were done in a collision cell using the gas modus with a helium gas flux of 1 mL min^{-1} due to the high concentrations while P was measured in normal mode.

Optical spectroscopy

UV/vis/NIR absorbance spectra were measured using a Cary 5000 spectrophotometer by Agilent Technologies in transmission mode. The samples were diluted with toluene and placed in a quartz glass cuvette (1 cm path length). In case of the nickel sulphide samples, this was done under an inert atmosphere.

X-ray diffraction

X-ray diffraction measurements were conducted employing a Bruker D8 Advance device in reflection mode. It was operated at 40 kV and 40 mA using Cu K-alpha radiation. The samples were purified analogously to the preparation for the TEM analysis. The nanoparticle dispersions in chloroform were then drop-casted onto and dried on a single crystalline silicon sample holder.

X-ray photoelectron spectroscopy

X-ray photoelectron spectroscopy measurements were conducted in a PHI Versaprobe II Scanning ESCA Microprobe (Physical Electronics) using a monochromatised Al K_α X-ray source (beam diameter 200 μm, X-ray power of 50 W). The analyser pass energy for detail spectra was set to 23.5 eV with a step time of 50 ms and a step size of 0.2 eV. During measurement, the sample was flooded with slow electrons and argon ions using the built-in ion sputter and electron guns in order to compensate surface charging effects. Data evaluation was performed using CasaXPS software. For the charge correction, the energy of the C 1s-line was set to 284.8 eV. The samples were prepared by iterative drop-casting of sample dispersions, which were cleaned analogously to the TEM and XRD sample preparations, on a 4 mm × 4 mm glass substrate.

Conflicts of interest

There are no conflicts to declare.

Acknowledgements

D. H. and D. D. are grateful for financial support by the German Research Foundation (DFG research Grant DO 1580/5-1). D. D. is furthermore funded by the DFG under Germany's Excellence Strategy within the Cluster of Excellence PhoenixD (EXC 2122, Project ID 390833453). R. H. acknowledges funding by the Hannover School for Nanotechnology (HSN). A. W. is thankful for financial support by the Deutsche Bundesstiftung Umwelt (DBU) in the form of a Promotionsstipendium (no. 20017/484). The authors would also like to thank the Laboratory of Nano and Quantum Engineering (LNQE) for the use of the TEM, Armin Feldhoff and Jürgen Caro for the use of the XRD, Anja Schlosser for additional TEM measurements as well as Andreas Breuksch for his assistance during the synthesis of some of the nanoparticle batches and Sven Getschmann for his help with the photographs.

References

1 T. Ishizaki, K. Yatsugi and K. Akedo, *Nanomaterials*, 2016, **6**, 172.

 This journal is © The Royal Society of Chemistry 2019

Open Access Article. Published on 24 July 2019. Downloaded on 2/7/2026 11:27:34 PM.
This article is licensed under a Creative Commons Attribution-NonCommercial 3.0 Unported Licence.

2 A. Sharma, J. Hickman, N. Gazit, E. Rabkin and Y. Mishin, *Nat. Commun.*, 2018, **9**, 1–9.
3 A. Vivien, M. Guillaumont, L. Meziane, C. Salzemann, C. Aubert, S. Halbert, H. Gérard, M. Petit and C. Petit, *Chem. Mater.*, 2019, **31**, 960–968.
4 S. Carenco, S. Labouille, S. Bouchonnet, C. Boissière, X. F. Le Goff, C. Sanchez and N. Mézailles, *Chem. – Eur. J.*, 2012, **18**, 14165–14173.
5 N. Cordente, M. Respaud, F. Senocq, M.-J. Casanove, C. Amiens and B. Chaudret, *Nano Lett.*, 2001, **1**, 565–568.
6 Y. Leng, Y. Zhang, T. Liu, M. Suzuki and X. Li, *Nanotechnology*, 2006, **17**, 1797–1800.
7 Y. Leng, Y. Li, X. Li and S. Takahashi, *J. Phys. Chem. C*, 2007, **111**, 6630–6633.
8 A. P. Lagrow, B. Ingham, S. Cheong, G. V. M. Williams, C. Dotzler, M. F. Toney, D. A. Jefferson, E. C. Corbos, P. T. Bishop, J. Cookson and R. D. Tilley, *J. Am. Chem. Soc.*, 2012, **134**, 855–858.
9 L. M. Moreau, D.-H. Ha, C. R. Bealing, H. Zhang, R. G. Hennig and R. D. Robinson, *Nano Lett.*, 2012, **12**, 4530–4539.
10 L. M. Moreau, D.-H. Ha, H. Zhang, R. Hovden, D. A. Muller and R. D. Robinson, *Chem. Mater.*, 2013, **25**, 2394–2403.
11 A. P. Lagrow, B. Ingham, M. F. Toney and R. D. Tilley, *J. Phys. Chem. C*, 2013, **117**, 16709–16718.
12 F. Gerdes, E. Klein, S. Kull, M. M. Ramin Moayed, R. Lesyuk and C. Klinke, *Z. Phys. Chem.*, 2018, **232**, 1267–1280.
13 S. Ghosh and L. Manna, *Chem. Rev.*, 2018, **118**, 7804–7864.
14 S. Zhang, G. Jiang, G. T. Filsinger, L. Wu, H. Zhu, J. Lee, Z. Wu and S. Sun, *Nanoscale*, 2014, **6**, 4852–4856.
15 S. Carenco, C. Boissière, L. Nicole, C. Sanchez, P. Le Floch and N. Mézailles, *Chem. Mater.*, 2010, **22**, 1340–1349.
16 J. Wang, A. C. Johnston-Peck and J. B. Tracy, *Chem. Mater.*, 2009, **21**, 4462–4467.
17 M. Zhou, Y. Kang, K. Huang, Z. Shi, R. Xie and W. Yang, *RSC Adv.*, 2016, **6**, 74895–74902.
18 S. E. Habas, F. G. Baddour, D. A. Ruddy, C. P. Nash, J. Wang, M. Pan, J. E. Hensley and J. A. Schaidle, *Chem. Mater.*, 2015, **27**, 7580–7592.
19 D. Hinrichs, R. Himstedt and D. Dorfs, *Nanoscale*, 2018, **10**, 9899–9907.
20 J. G. Railsback, A. C. Johnston-Peck, J. Wang and J. B. Tracy, *ACS Nano*, 2010, **4**, 1913–1920.
21 R. Himstedt, P. Rusch, D. Hinrichs, T. Kodanek, J. Lauth, S. Kinge, L. D. A. Siebbeles and D. Dorfs, *Chem. Mater.*, 2017, **29**, 7371–7377.
22 R. Himstedt, D. Hinrichs and D. Dorfs, *Z. Phys. Chem.*, 2018, **233**, 3–14.
23 T. Iwamoto, A. Nagao, K. Kitagishi, S. Honjo and B. Jeyadevan, *J. Phys. Chem. Solids*, 2015, **87**, 136–146.
24 H. Winnischofer, T. C. R. Rocha, W. C. Nunes, L. M. Socolovsky, M. Knobel and D. Zanchet, *ACS Nano*, 2008, **2**, 1313–1319.
25 Y. Tan, D. Sun, H. Yu, B. Yang, Y. Gong, S. Yan, Z. Chen, Q. Cai and Z. Wu, *CrystEngComm*, 2014, **16**, 9657–9668.
26 J. Park, E. Kang, S. U. Son, H. M. Park, M. K. Lee, J. Kim, K. W. Kim, H. J. Noh, J. H. Park, C. J. Bae, J. G. Park and T. Hyeon, *Adv. Mater.*, 2005, **17**, 429–434.
27 K. Mandel, F. Dillon, A. a. Koos, Z. Aslam, K. Jurkschat, F. Cullen, A. Crossley, H. Bishop, K. Moh, C. Cavelius, E. Arzt and N. Grobert, *Chem. Commun.*, 2011, **47**, 4108–4110.
28 H. P. Andaraarachchi, M. J. Thompson, M. A. White, H. J. Fan and J. Vela, *Chem. Mater.*, 2015, **27**, 8021–8031.
29 S. Carenco, Y. Hu, I. Florea, O. Ersen, C. Boissière, N. Mézailles and C. Sanchez, *Chem. Mater.*, 2012, **24**, 4134–4145.
30 J. Contreras-Mora, H. Ariga-Miwa, S. Takakusagi, C. T. Williams and K. Asakura, *J. Phys. Chem. C*, 2018, **122**, 6318–6322.
31 E. Muthuswamy, G. H. L. Savithra and S. L. Brock, *ACS Nano*, 2011, **5**, 2402–2411.
32 D. Li, K. Senevirathne, L. Aquilina and S. L. Brock, *Inorg. Chem.*, 2015, **54**, 7968–7975.